A novel thin-film nano-templated composite membrane with *in situ* silver nanoparticles loading: Separation performance enhancement and implications

Zhe Yang[a], Yichao Wu[b,c], Hao Guo[a], Xiao-Hua Ma[a,d], Chun-er Lin[e],Ying Zhou[a], Bin Cao[b,c], Bao-ku Zhu[e], Kaimin Shih[a], Chuyang Y. Tang[a,*]

[a] Department of Civil Engineering, the University of Hong Kong, Pokfulam, Hong Kong

[b] School of Civil and Environmental Engineering, Nanyang Technological University, 50 Nanyang Avenue, Singapore 639798

[c] Singapore Centre for Environmental Life Sciences Engineering, Nanyang Technological University, 60 Nanyang Avenue, Singapore 637551

[d] School of Chemical Engineering, East China University of Science and Technology, Mei Long Road 130, Shanghai 200237, P. R. China

[e] ERC Membrane and Water Treatment Technology (MOE), Department of Polymer Science and Engineering, Zhejiang University, Hangzhou 310027, P. R. China

[*] To whom correspondence should be sent,

Address: HW 6-19b, Haking Wong Building, Pokfulam Road, Department of Civil Engineering, The University fo Hong Kong, Hong Kong SAR, China

Tel: +852 2859 1976,

Fax: +852 2559 5337,

E-mail address: tangc@hku.hk

Abstract

We developed a facile approach to synthesize thin-film nano-templated composite (TFNt) nanofiltration membrane with high water permeability, high NaCl/$MgSO_4$ selectivity and strong antimicrobial properties. A polydopamine (PDA) coating on a polysulfone support was used as a nano-template to generate silver nanoparticles (AgNPs) *in situ* with high loading and high uniformity. A subsequent interfacial polymerization reaction of piperazine and trimesoyl chloride was performed on this nano-template substrate to form the TFNt membrane. The TFNt membrane had significantly increased both the water permeability and salt rejection than the control thin-film composite (TFC) membrane as well as a thin-film nanocomposite (TFN) membrane prepared the conventional way of loading AgNPs directly during the interfacial polymerization process. Furthermore, the TFNt membrane showed better antimicrobial properties than both the TFC and the conventional TFN membranes. The current work presents an exciting approach to fabricate novel nanofiltration membranes using nano-templates, which provides important insights for high performance NF membrane synthesis.

Keywords: Nanofiltration; nanocomposite membrane; nano-template; water permeability; selectivity.

47 Graphical Abstract

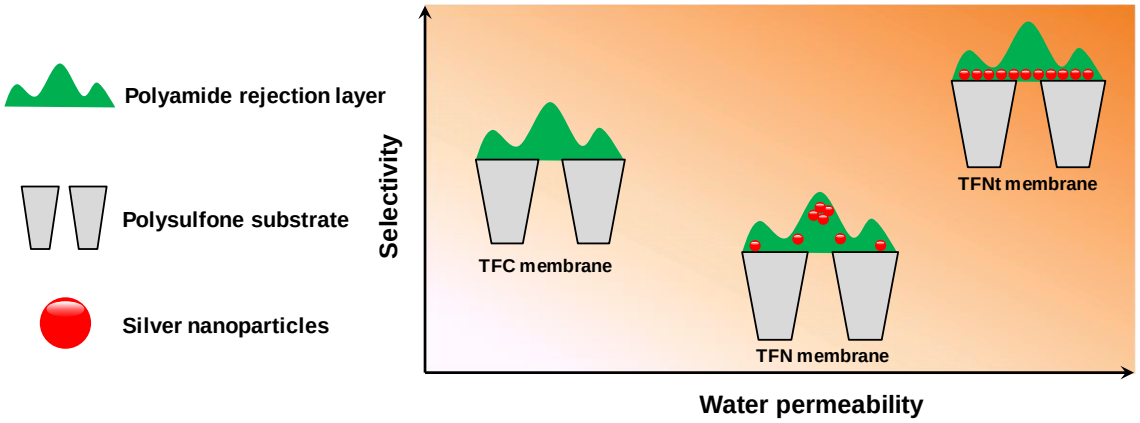

48

49

1. Introduction:

Nanofiltration (NF) membranes, with characteristic pore size on the order of 1 nm, have been applied in surface water treatment (e.g., for the removal of natural organic matter and disinfection by-products) [1, 2], wastewater reclamation [3, 4], industrial wastewater treatment (e.g., dye removal) [5-7] and seawater pretreatment [8, 9]. An ideal NF membrane should have high water permeability, high solute selectivity and good antifouling properties [10]. One widely used chemistry for the NF rejection layer is polyamide, which is formed by the interfacial polymerization (IP) of an acid chloride monomer and an amine monomer [11]. In recent years, many research groups have focused on the development of thin-film nanocomposite (TFN) membranes, in which nanoparticles (NPs) are incorporated in the polyamide rejection layer to improve their separation and antifouling performance [12-14]. Examples of nanomaterials used for TFN membrane preparation include zeolite nanoparticles [12, 13], TiO_2 [15], silver [16, 17], silica [18], carbon nanotubes [19-21] and graphene oxide [22, 23].

A key challenge for the preparation of TFN membranes is the aggregation of NPs, which can prevent the effective loading of NPs and adversely affect membrane separation performance. For example, Wu et al. [19] incorporated multiwall carbon nanotubes (MWNTs) to aqueous amine solution during interfacial polymerization. Although water permeability improved upon initial increase in MWNTs loading (up to 0.5 g/L), further increase in loading led to a reduction in both permeability and salt rejection. They attributed the inferior membrane performance to the agglomeration of MWNTs, which hindered the formation of densely-crosslinked rejection layer [19]. Likewise, Yin et al.

[24] found that water permeability first increased and then leveled off at higher concentration mesoporous silica NPs (MCM-41) due to their severe aggregation. Recently, Dong et al. [25] pre-loaded zeolite NPs onto a PSF support through phase inversion in an aqueous solution containing zeolite NPs. Whereas their approach addresses the issue of NPs aggregation, the lack of strong chemical bonding between zeolite NPs and the PSF support may result in a weak mechanical stability of the resulting rejection layer. Therefore, a more efficient technique to make stable and high performance nanocomposite membranes is required.

We envisage a nano-templated structure, which can further grow NPs *in situ* with excellent uniformity and high loading. An interesting candidate is polydopamine (PDA) [26], a mussel-inspired coating material that can firmly attach onto support layer with excellent stability. Its catechol groups can further reduce silver ions to form uniformly-distributed silver nanoparticles [27]. In the current study, we performed interfacial polymerization on a PDA/Ag treated substrate to form a novel thin-film nano-templated composite (TFNt) membrane. Its separation performance and antibacterial properties were compared with conventional TFN membranes formed by directly dispersing AgNPs during IP process.

2. Methods

2.1. Materials and reagents

Unless described otherwise, all solutions were prepared from analytical-grade chemicals and Millipore ultrapure water. Polysulfone (PSF, Mw 35,000), Dimethylformamide (DMF, anhydrous 99.8%), silver nitrite ($AgNO_3$, ACS agent >99.0 %), piperazine (PIP, ReagentPlus®, 99%), trimesoyl chloride (TMC, 98%), sodium chloride (NaCl, >99.5%) and magnesium sulfate ($MgSO_4$, ReagentPlus® >99.5%) were all obtained from Sigma-Aldrich. Dopamine hydrochloride (J&K Scientific Ltd., China), Tris (hydroxymethyl, Acros Organics, Geel, Belgium) and hydrochloric acid (HCl, 37 wt %, VWR, Dorset, U.K) were used for the preparation of PDA coatings. AgNPs (>99.95%, particle size of 20-30 nm) was purchased from SkySpring nanomaterials (Houston, TX) to prepare conventional TFN membranes for comparison purpose.

2.2. Synthesis of PSF support layers

The PSF support layer was prepared by the phase inversion method according to our previous work [28]. A 15 wt% PSF solution was prepared by dissolving PSF pellets in DMF, and the solution was then stirred and heated at 50 °C overnight for degassing. A thin polymer film was casted by spreading the PSF dope onto a glass plate by a casting knife (EQ-Se-KTQ-150, MTI Corp., Richmond, CA) at a gate height of 150 μm. The casted film was immersed in a deionized water bath at 25 °. The resulting PSF support membrane was rinsed and kept in DI water for at least 24 h before further use.

2.3. Synthesis of TFNt membranes

In the current study, we utilized PDA as a nano-template to immobilize AgNPs on the PSF substrate, which was followed by an interfacial polymerization reaction to form the final nanocomposite membrane (denoted as thin film nano-templated composite or TFNt, see Figure 1). Procedures for preparing the PDA coating and AgNPs immobilization were adapted from our previous work [26]. A PSF coupon of 20 × 12 cm was placed in a custom-made container to expose its skin side to the coating solution (2 g/L dopamine hydrochloride in a 10 mM Tris-HCl buffer solution at pH=8.5) for one hour to form the PDA coated substrate. AgNPs were formed *in situ* by soaking this coated substrate in a 4g/L $AgNO_3$ solution for 5 h (room temperature, in the dark and under continuous shaking). The PDA-coated PSF substrate is denoted as PDA-PSF, and the Ag loaded substrate is named as PDA/Ag-PSF.

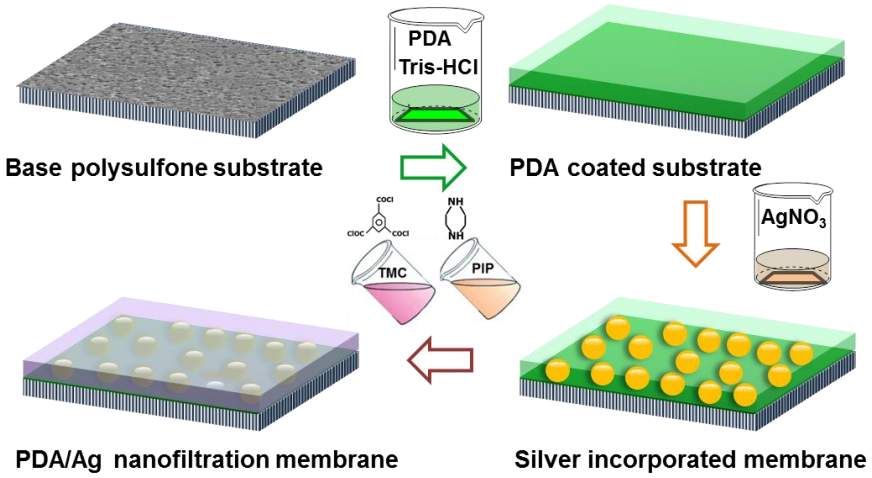

Fig. 1. A schematic diagram showing the synthesis of thin film nano-templated composite (TFNt) membrane. A polysulfone substrate was first coated with polydopamine, followed by *in situ* reduction of silver by immersing it into an $AgNO_3$ solution. An interfacial polymerization of PIP and TMC onto the PDA/Ag treated substrate forms the TFNt membrane, in which AgNPs uniformly distributed in its

composite rejection layer.

To fabricate the TFNt membranes, the PDA/Ag-PSF substrate was rinsed with DI water and then immersed in a 100 ml 2.0 wt% PIP/water solution for 3 min. Excess solution was removed by a rubber ruler. Then, a 25 ml 0.15 wt% TMC/hexane solution was poured onto the PIP soaked substrate and the reaction was continued for 1 min to form the PA thin-film rejection layer. The resultant membrane (TFNt) was rinsed with hexane and post-treated in an oven at 60 °C for 10 min, and then stored in DI water at 4 °C for at least 12 h before further use. PDA1h-TFC membranes were also fabricated in a similar manner except the silver loading step was skipped. This membrane was used as a control to resolve the role of PDA and AgNPs on the membrane transport properties.

2.4. Synthesis of the TFC and TFN membranes

Control TFC and TFN membranes were fabricated using the PSF substrate directly. The TFC membrane contained no AgNPs. For the synthesis of TFN, 0.05 (w/v)% AgNPs were loaded in the TMC/hexane solution. This loading amount is optimized based on reported literature [29, 30]. According to their findings, higher AgNPs loading may cause severe disruption to the PA rejection layer. To obtain a good AgNPs dispersion, the mixtures of AgNPs and TMC/hexane solution were ultrasonicated for at least 1 h before IP. The other procedures for the interfacial polymerization were identical to those as described in Section 2.3.

157 *2.5. Membrane characterization*

158 Membrane functional groups were assessed by attenuated total reflection Fourier
159 transform infrared (ATR FTIR) spectroscopy with a Nicolet 6700 FTIR spectroscope
160 (Thermo Fisher Scientific, Waltham, MA) over a wave numbers from 650 to 4000 cm^{-1} at
161 a resolution of 2 cm^{-1}.

162

163 The surface elemental compositions of the membranes were assessed by an X-ray
164 photoelectron spectroscopy (XPS) using an SKL-12 spectrometer (Leybold, Sengyang,
165 China) with a VG CLAM 4 MCD electron energy analyzer. An Al Kα gun (1496.3 eV)
166 operated at 10 kV and 15 mA was applied as the x-ray source. Survey spectra over 0-
167 1000 eV were acquired at a scanning resolution of 0.1 eV. Membrane testing samples
168 were thoroughly rinsed several times and dried before XPS characterization.

169

170 Scanning electron microscopic characterization was obtained by scanning electron
171 microscope (SEM, LEO 1530 FEG, UK) with an energy dispersive spectroscopy (EDS)
172 detector. Membrane samples (0.5 × 0.5 cm) were vacuum-dried and sputter-coated with a
173 uniform layer of gold and platinum (SCD 005, BAL-TEC, NYC). SEM images were
174 acquired at an accelerating voltage of 5 kV. EDS was also assessed at a voltage of 20 kV.

175

176 For transmission electron microscopic (TEM) characterization, both membrane cross
177 sections and isolated PA rejection layers were investigated. To obtain an isolated PA thin-
178 film, a small NF coupon (< 2 x 2 mm) was immersed into a DMF solvent to dissolve its
179 PSF substrate. The resulting PA thin-film, floating in the DMF solvent, was picked up by
180 a carbon-coated copper TEM grid and dried in air. Membrane cross-section samples were

prepared by embedding the NF membrane in an Epon resin (Eponate 12, Ted Pella, CA) and were cut by Reichert-Jung Ultracut E ultramicrotome (Reichert, Inc. Depew, NY) into ultrathin sections (thickness around 100 nm). All samples were performed with Philips CM100 TEM (Philips, Eindhoven, Netherlands) operating at 100 kV.

Atomic force microscopy (AFM, Veeco, Nanoscope IIIa Multimode) was applied to exam the surface roughness of membrane, in which *rms* (root-mean-square roughness) were analyzed by software Nanoscope Analysis (Bruker, MA) with 5 μm × 5 μm scanning range.

Streaming potential (SurPASS 3 Electrokinetic Analyzer, Anton PaarGmbH, Austria) was used to test the surface charge over a pH range of 3-10 using 1.0 mM KCl as background electrolyte solution. Water contact angle were obtained using a goniometer equipped with a video capture device (Powereach®, China). Before each test, a membrane sample was dried in vacuum at room temperature for 24 h. A DI water droplet with a volume of approximately 5 μL was placed on the membrane surface with a stabilizing time of 10 seconds. For each membrane sample, contact angle was measured at five different places and the average value was calculated.

2.6. Separation performance testing

A high pressure cross-flow filtration system, similar to the one reported by Yang et al. [28] was used to evaluate water flux and solute rejection of membranes under a constant pressure mode. The temperature was kept at 24 ± 0.5 °C using an immersion thermostat (J.P. Selecta S.A., Barcelona, Spain). For each test, a membrane coupon with an effective

area of 13.4 cm^2 was placed in a filter holder (model: XX4504700, stainless steel, Millipore Corp., Billerica, MA). The coupon was pre-compacted using DI water at the set pressure of 1 MPa for 2 h in order to achieve a stable water flux. The pure water flux was then calculated by measuring the mass of the permeate water collected over a specified time interval according to Equation (1):

$$J_v = \frac{\Delta w}{\Delta t \times A \times \rho} \quad (1)$$

where J_v (L/ (m^2 h) is the water flux, Δw (kg) is the mass of permeate water collected over a time period of Δt (h), A (m^2) is the effective membrane area, and ρ (kg/L) is the density of permeate water.

Salt rejection was measured using a 1000 ppm $MgSO_4$ or NaCl solution as the feed water. An Ultrameter II (Myron L company, Carlsbad, CA) was used to determine the conductivity of the feed water (C_f) and that of the permeate (C_p), respectively. Membrane rejection R was calculated by Equation (2) and the separation factor (α) of NaCl to $MgSO_4$ was determined by Equation (3):

$$R = (1 - \frac{C_p}{C_f}) \times 100\% \quad (2)$$

$$\alpha = \frac{(C_{NaCl} / C_{MgSO_4})_p}{(C_{NaCl} / C_{MgSO_4})_f} = \frac{1 - R_{NaCl}}{1 - R_{MgSO_4}} \quad (3)$$

2.7. Antimicrobial performance evaluation

All membranes samples were stored in DI water for 24 h before antimicrobial tests. A

Gram-positive *Bacillus subtilis* 168 (ATCC 27370) and a Gram-negative *Escherichia coli* K12 (ATCC 10798) were used as the model bacteria [31]. Membrane samples were placed in the cell suspension and then cultivated on a rotary shaker (150 rpm) at room temperature (10 h for *B. subtilis* and 24 h for *E. coli*). Viable cells were determined using the colony forming unit (CFU) method (CLSI M07-A935) [32].

Diffusion inhibition zone (DIZ) tests were performed based on previous work [26]. Aliquots around approximately 100 μL of bacterial culture were spread onto LB agar plates. Membrane disk samples (diameter = 12.7 mm) were then placed onto the plate with their rejection layers facing the agar surface. After incubation at optimal temperature (30 ºC for *B. subtilis* and 37 ºC for *E. coli*) for 24 h, the bacterial slime developed under the membrane samples was examined.

2.8. Quantifying of silver loading and silver leaching tests

To measure the total amounts of silver on the membrane samples, AgNPs functionalized membrane coupons (1.13 cm^2) were immersed in plastics vials containing 0.2 ml 70% HNO_3 in 20 ml DI water. The vials were shaken under 200 rpm for three days. The dissolved silver concentration was quantified using an inductive coupled plasma optical emission spectrometer (ICP-OES, Optima 8×00, Perkin Elmer). The stability of AgNPs in the TFNt membrane was assessed on the basis of dynamic flow-through silver leaching tests (Supporting Information Appendix D).

3. Results and Discussion

3.1. ATR FTIR results

ATR FTIR spectrum of the PSF substrate showed several characteristic peaks (Figure 2): 1587, 1504 and 1488 cm^{-1} attributed to aromatic C-C stretching, 1320 and 1280 cm^{-1} to the doublet from asymmetric sulfone group (O=S=O), 1245 cm^{-1} to the asymmetric C-O-C stretching of aryl ether group and 1160 cm^{-1} to the symmetric stretching of sulfone group [10, 33]. No additional major peaks were found for the PDA/Ag-PSF membrane (Figure 2b), which can be explained by the very thin thickness of PDA coating (about 10 nm) [34]. In contrast, TFNt and TFC membranes had additional peaks at around 1630 cm^{-1} attributed to the Amide I band for poly(piperazinamide) and 1434 cm^{-1} assigned to C-N bond [10, 35].

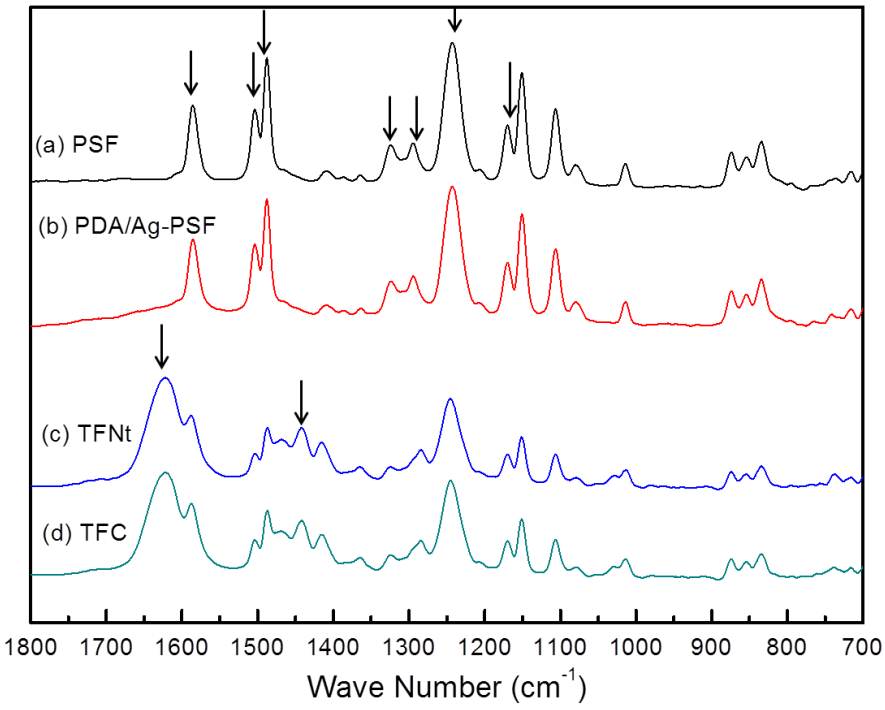

Fig. 2. ATR FTIR spectra of PSF, PDA/Ag-PSF, TFNt, and TFC. Both TFNt and TFC were formed with a PIP concentration of 2 wt% and TMC concetration of 0.15 wt%.

3.2. Membrane SEM, TEM morphological images and AFM roughness results

Figure 3 shows the SEM micrographs of PSF, PDA/Ag-PSF, TFC, TFNt and TFN and the TEM micrographs of TFC, TFNt and TFN. The PSF substrate (Figure 3a) had a relatively smooth surface with nano-sized pores of 32.1 ± 5.4 nm (analyzed by Image-Pro Plus 6.0, MediaCybernetics, Inc.). After silver immobilization, fine particles (diameter ~ 27.8 ± 4.7 nm) were observed on the PDA/Ag-PSF substrate (Figure 3b). EDS analysis (Figure A2) further confirmed that these fine particles were AgNPs. The TFC membrane (Figure 3c) had a nodular surface morphology that is typical for the PIP/TMC interfacial chemistry [36]. In the SEM plan view of the TFNt membrane (Figure 3d), a similar nodular morphology interfered the identification of AgNPs. In contrast, a comparison of the TEM plan views of TFC (Figure 3e) and TFNt (Figure 3f) confirmed the presence of AgNPs in the TFNt membrane. Both Figure 3b and Figure 3f show that these silver nanoparticles were uniformly distributed, with estimated plan coverage as high as 25.0 ± 1.1%. In addition, both SEM and TEM of the TFN membrane showed the aggregation of AgNPs.

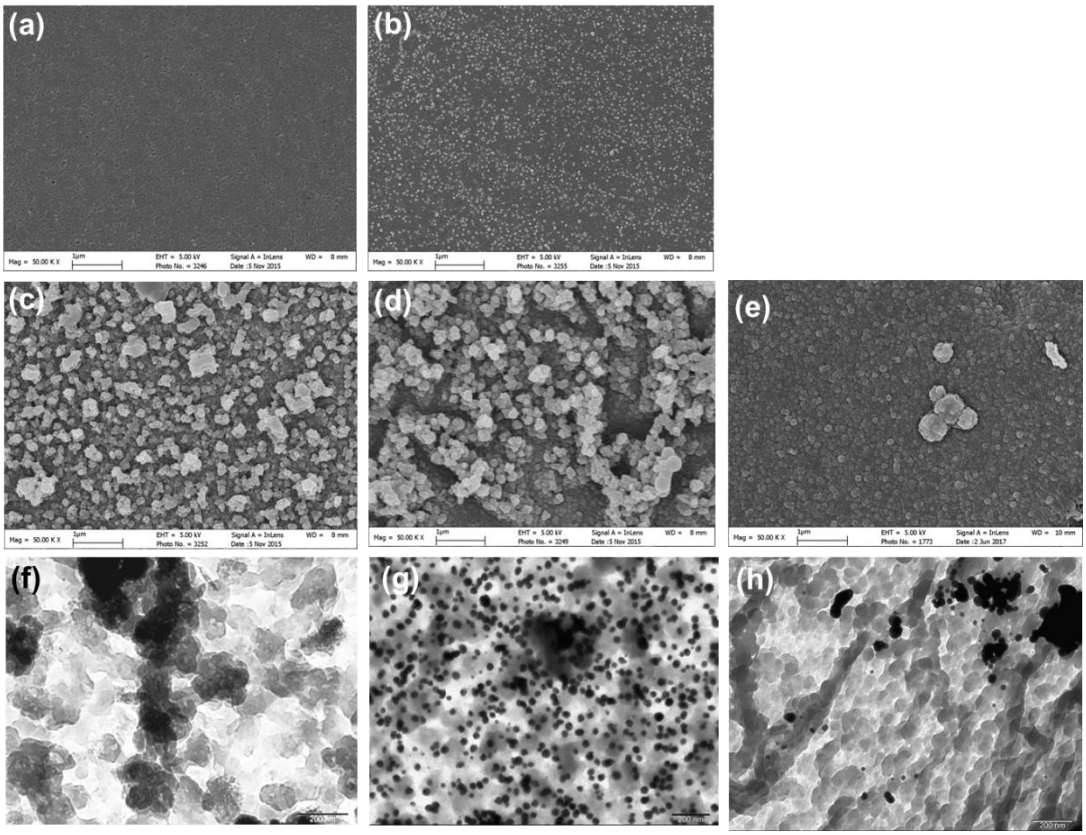

Fig. 3. SEM micrographs (plan view) of (a) the control PSF substrate, (b) the silver incorporated PDA/Ag-PSF substrate, (c) the TFC membrane, (d) the TFNt membrane, (e) the TFN membrane; TEM micrographs (plan view) of (f) TFC, (g) TFNt and (h) TFN. Both TFNt, TFN and TFC were formed with a PIP concentration of 2 wt% and TMC concentration of 0.15 wt%. The scale bars for SEM and TEM are 1 μm and 200 nm, respectively.

TEM cross-section images of the TFC, TFNt and TFN membranes are presented in Figure 4. While the control TFC membrane (Figure 4a) contained no AgNPs, both the nano-templated TFNt (Figure 4b) and the conventional TFN (Figure 4c) had AgNPs successfully incorporated. Since the AgNPs were immobilized in the PDA nano-template, these particles appeared at the bottom (substrate side) of the rejection layer. In contrast to the orderly templated AgNPs that were uniformly distributed in the polyamide rejection layer of TFNt, the AgNPs in the conventional TFN membrane appeared to be highly non-uniformly distributed. Severe particle agglomeration occurred at the surface of the

polyamide rejection layer, which could not only adversely affect its rejection [37] but also increase the risk of AgNPs detachment. The silver loading in TFNt appeared to be much higher compared to that in TFN, which is further confirmed by additional silver leaching analysis (silver loading = 14.7 ± 2.2 μg/cm^2 for TFNt and 3.2 ± 0.4 μg/cm^2 for TFN). Indeed, the conventional TFN membrane had a rather low silver loading efficiency: only about 6% of the AgNPs added in the TMC/hexane solution (52.1 μg/cm^2) was effectively incorporated in the final membrane. In contrast, the silver loading efficiency of the TFNt membrane was approximately 30%, which was significantly higher than that of the TFN membrane (approximately 6.1%, Table 1). The enhanced silver loading and particle distribution resulting in TFNt from the nano-templating approach are expected to improve the separation performance of the resulting membrane.

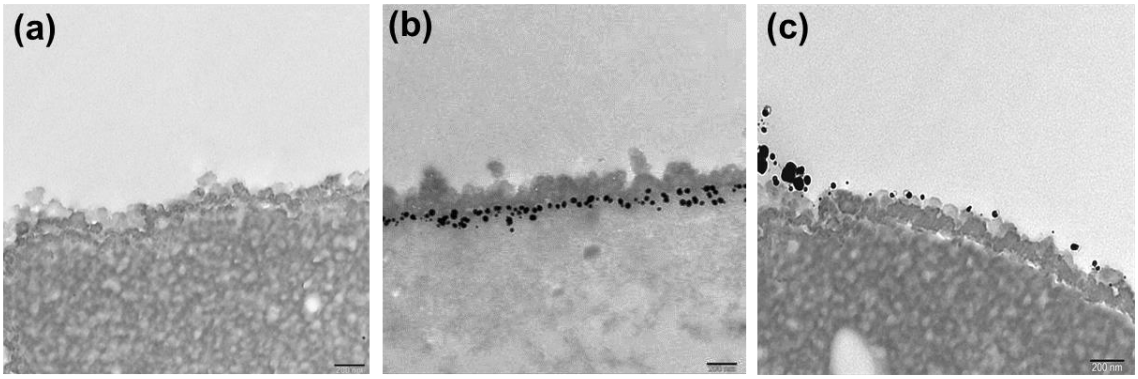

Fig. 4. TEM micrographs (cross-sections) of (a) the TFC, (b) the TFNt, and (c) the TFN membranes The scale bar of all TEM images is 200 nm.

AFM was applied to investigate membrane surface morphology and roughness. The base PSF substrate and the PDA-coated PDA-PSF substrate (Figure 5a,b) had relatively low RMS roughness (R_q=8.9 nm for PSF and 11.1 nm for PDA-PSF). Silver loading increase the substrate roughness to 18.6 nm (PDA/Ag-PSF, Figure 5c). Consistently, the silver-

incorporated nano-templated TFNt membrane had a slightly rougher surface (R_q = 113 nm, Figure 5d) compared to the control TFC membrane (R_q = 98.8 nm, Figure 5e). The conventional TFN membrane had the highest surface roughness of 130 nm (Figure 5f), likely due to the agglomeration of AgNPs on the membrane surface (Figure 4c).

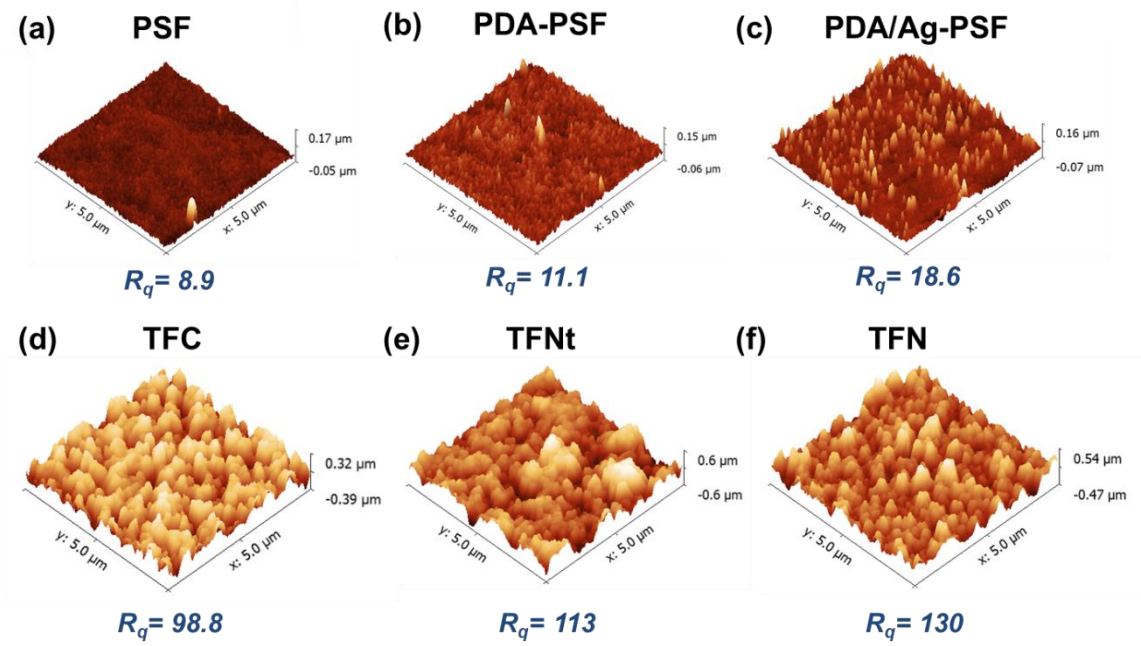

Fig. 5. AFM microimages of PSF, PDA-PSF, PDA/Ag-PSF, TFC, TFNt and TFN. The root mean square (R_q) roughness value of each membrane is also shown at the bottom.

3.3. Membrane surface properties and separation performances

The contact angles of the TFC and TFNt membranes were comparable (32.8 ± 1.8 and 33.5 ± 3.1°, respectively; see Table 1). In contrast, TFN had a much lower contact angle of 21.3 ± 3.2 °. Its reduced contact angle is attributed to the hydrophilic nature of AgNPs [30, 38]. Based on our TEM characterization (Figure 4), the AgNPs of TFN are largely exposed on the surface, while those of TFNt are shielded by the polyamide rejection layer. XPS analysis show a similar O:N ratio 1.6-1.7 for TFC and TFNt (also see

Supporting information Appendix A). In comparison, a much higher ratio of 2.1 was measured for TFN, which implies a greatly reduced crosslinking degree for the conventional TFN membrane [37]. In this respect, the increased O:N ratio for TFN may result from the hydrolysis of –COCl groups with water attached to the hydrophilic AgNPs to form oxygen rich $–COO^-$, causing a disrupted polyamide structure. In addition, the PDA1h-TFC membrane (without AgNPs) did not show significant difference in its contact angle and O:N ratio compared to the respective values of the control TFC membrane.

Table 1. Membrane contact angles, separation Performance, XPS of O:N ratio on membranes surface and silver loading amounts and efficiency.

Membrane	Contact angle (°)	Permeability (L/(m^2 h bar)[a]	$MgSO_4$ rejection (%)[a]	NaCl rejection (%)[a]	α (NaCl/MgSO4)[b]	O:N ratio (XPS)[d]	Loaded silver amounts (μg/cm^2)[e]	AgNPs loading efficiency (%)[f]
Control-TFC[c]	32.8 ± 1.8	2.8 ± 0.4	97.7 ± 0.9	43.9 ± 3.3	24.4 ± 3.5	1.6	0	0
PDA1h-TFC	31.6 ± 2.1	4.7 ± 0.4	98.1 ± 0.3	47.5 ± 2.3	27.3 ± 2.8	1.5	0	0
TFNt[c]	33.5 ± 3.1	5.9 ± 1.8	98.5 ± 0.4	47.1 ± 4.8	35.3 ± 5.8	1.7	14.7 ± 2.2	30.2 ± 4.6
TFN[c]	21.3 ± 3.2	5.1 ± 0.9	95.2 ± 0.5	38.7 ± 1.3	12.7 ± 1.2	2.1	3.2 ± 0.4	6.1 ± 0.8

Note:

[a] Experimental condition: The pure water permeability was determined using DI water as the feed at 25 °C. Then, 1 g/L $MgSO_4$ or NaCl was added into the DI water feed solution and salt rejection was determined based on the measured conductivity values of feed and permeate solution. The experimental results were calculated from at least three replicate measurements.

[b] Separation factor (α) was determined by Equation (3).

[c] The monomer concentrations applied for the three types of membranes were at 2 wt% PIP with 0.15 wt% TMC.

[d] O:N ratio was calculated based on the XPS results of O and N atomic concentration on membrane PA surface.

[e] Effective silver loading was measured by placing 1.13 cm^2 membrane samples into 20 ml HNO_3 solution.

[f] AgNPs loading efficiency was calculated by the actual silver loading on the basis of ICP results divided by the initial amount of the silver used for membrane fabrication.

The water permeability of both TFNt and TFN significantly improved compared to that of the control TFC (82% enhancement for TFN membrane and 110% for TFNt). On the

other hand, different trends were observed for the salt rejection and selectivity. Whereas TFN suffered from a decreased salt rejection, the nano-templated TFNt showed improved rejection of $MgSO_4$ and NaCl as well as the NaCl/$MgSO_4$ selectivity. In general, the shift in separation performance can be explained by several reasons:

- *The hydrophilicity of the nanoparticles (NPs)*. Embedding hydrophilic nanoparticles are known to enhance water permeability [37]. The much hydrophilic nature of AgNPs compared to the polyamide matrix (Table 1) explains the enhancement in water permeability.
- *Defects formation in the rejection layer*. In addition, the introduction of NPs in the polyamide matrix may result in interfacial gaps between the NPs and the matrix [39], leading to accelerated water permeation in these defects. These defects formation would also reduce the salt rejection, as for the case of TFN. The agglomeration of AgNPs may have promoted more defects in the resulting composite membrane [37]. XPS analysis provided further evidence of reduced crosslinking degree of the TFN membrane, which caused a compromised membrane selectivity.

Our results seem to suggest that TFNt had fewer defects, probably due to the more uniform distribution of AgNPs with the nano-templated approach. Its enhanced rejection could be partially explained by the dilution effect caused by the greater water permeability. In addition, the enhanced charge repulsion by the more negatively charged silver nanoparticles (Figure 6) may have contributed to the better rejection and NaCl/$MgSO_4$ selectivity. AgNPs generally exhibited negative charge due the surface oxidization [40, 41]. In addition, AgNPs may attract anions (e.g., Cl^- and citrate ions) on

379 their surface, which can further induce negative charge [42-44]. According to Donnan
380 exclusion theory, a more negative charged membrane will better repel anions and the
381 effect is strong for ions with great valence (i.e., SO_4^{2-} > Cl^-), leading to a stronger
382 enhancement for $MgSO_4$ rejection compared to NaCl rejection [36, 45]. Interestingly, the
383 PDA1h-TFC membrane also showed both enhanced water permeability and selectivity
384 compared to that of the control TFC membrane, which can be possibly explained by the
385 narrower distribution of the substrate pore size (i.e., less defects in the substrate) and
386 more hydrophilic chemical groups introduced by the polydopamine [36, 46]. In addition,
387 both water permeability and selectivity of the TFNt membrane were higher than that of
388 the PDA1h-TFC, potentially due to the hydrophilic nature of the AgNPs to enhance the
389 water diffusion in the polyamide rejection layer [37].
390
391

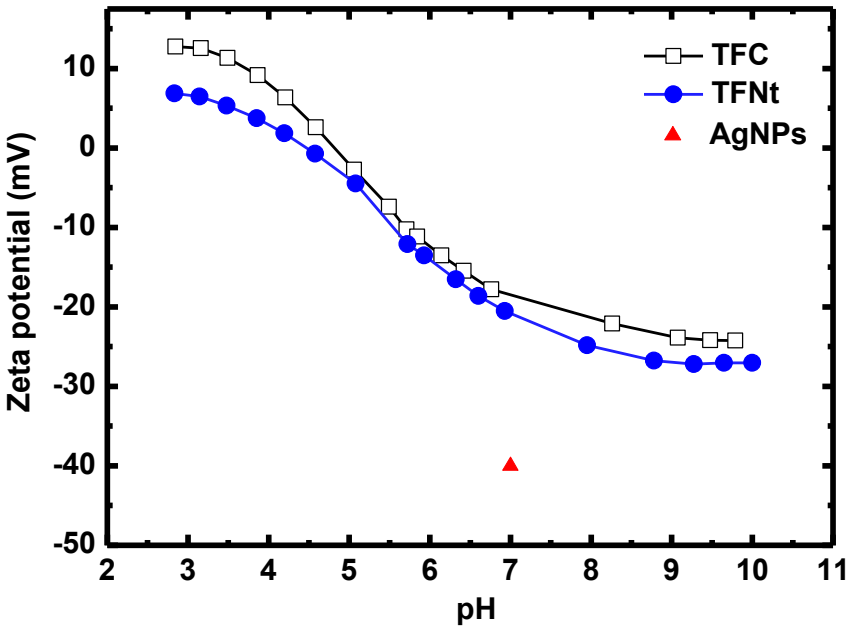

392
393 Fig. 6. Zeta potential of TFC and TFNt over a pH range of 3-10 by using 1.0 mM KCl as background
394 electrolyte solution. The zeta potential of AgNPs, obtained from [31], is also included in the figure for

comparison purpose.

3.4. Membrane antimicrobial results

AgNPs based nanocomposite membranes offer further advantage of antimicrobial effect [16, 26, 30, 47, 48]. DIZ and CFU experiments were conducted to evaluate the membranes' antibacterial properties. In DIZ tests, for both *B. subtilis* and *E. coli*, visible bacterial slime was developed under the silver-free control-NF membrane and the TFN membrane. In contrast, no apparent bacterial growth was observed for the TFNt membrane due to its much higher silver loading (see Figure 4 and Table 1). CFU tests also showed stronger antibacterial effects of the TFNt membrane (Figure 7), where the exposure to the TFNt membranes led to a significant reduction of viability by 90.1 ± 6.3% for *B. subtilis* and 44.4 ± 13.7% for *E. coli*. While for the TFN membrane, we barely observed any antibacterial effect, potentially due to its low loading amounts of AgNPs.

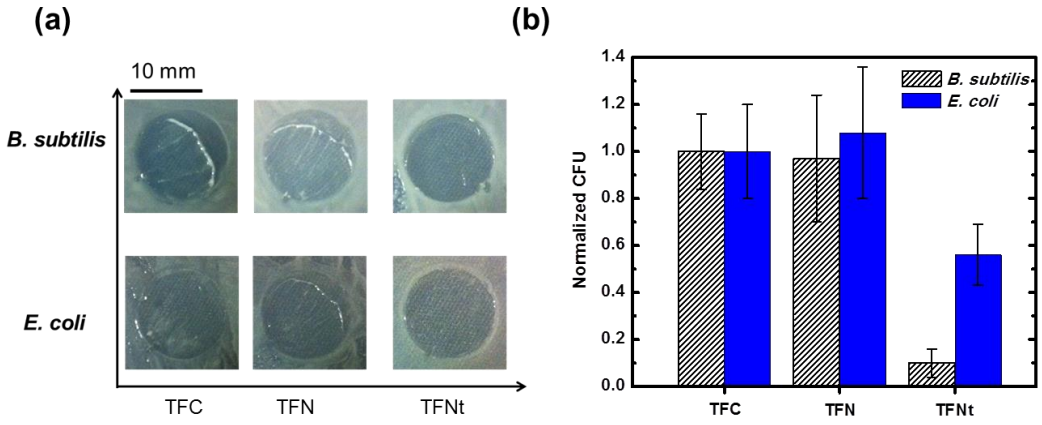

Fig. 7. (a) Antibacterial properties of TFC, TFN, and TFNt membranes. (a) Diffusion inhibition zone tests for Gram-positive *B. subtilis* and Gram-negative *E. coli*. Membrane coupons (diameter around 12 mm and rejection layer facing downward) were placed onto agar plates spread with bacterial culture

415 with 24 h incubation time. (b) Colony forming units tests for *B. subtilis* and *E. coli*. Membrane
416 coupons were placed into cell suspensions (cell density of approximately 3.0×10^7 cells/mL for *B.*
417 *subtilis* and 2.0×10^8 cells/mL for *E. coli*). The data presented are the average value of three
418 replicates.
419

3.5. Discussion

Table 2 summarizes the recently reported TFN membranes on the basis of types of nanofillers and the incorporation method. The enhancement is generally limited using conventional method, e.g., adding AgNPs into organic (TMC) phase or aqueous (PIP or other amines such as m-Phenylenediamine) as well as during layer-by-layer assembly. In particular, many studies on AgNPs reported no enhancement or even a reduction in salt rejection. For other types of nanofillers such as SiO_2, zeolite, multi-wall carbon nanotubes (MWCNTs) and graphene oxide (GO), several studies have also indicated the risk of rejection loss despite of the general trend of enhancement in water permeability. The deteriorated rejection is generally attributed to defects caused by nanofiller incorporation. Indeed, the existing literature has pointed to the critical importance of the dispersion of nanofillers in order to maintain the integrity of the membrane rejection layer [24, 37].

In the current study, we have synthesized high performance thin-film nano-templated composite (TFNt) membranes by preparing a silver functionalized PDA nano-template, followed by an interfacial polymerization reaction. The resulting TFNt membrane, with a 110% enhancement in water permeability combined by improved salt rejection, significantly outperformed both the control TFC and TFN membranes due to its high AgNPs loading with excellent uniformity. Future studies may further explore the *in situ* growth of other nanomaterials (e.g., TiO_2, SiO_2, and MOFs) as well as alternative templating methods for improved membrane performance.

443 Table 2. Comparison of recent thin-film nanocomposite NF membranes to this work.

Nanofiller	Polymer	Loading (wt.%)	Performance	Published year and Reference
AgNPs	PDA nanotemplate/PA	14.7 ± 2.2 μg/cm^2	Double the water permeability with ↑ salt rejection; Antimicrobial property ↑	This work
AgNPs	PA	3.2 ± 0.4 μg/cm^2	Pw ↑ by 82%; MgSO4 and NaCl rejection ↓	This work
AgNPs	PA	Dispersed in organic phase[a]	No major change in water flux and salt rejection; Antibiofouling property ↑	2007 [29]
AgNPs	PA	Dispersed in aqueous phase[a]	P_w↑ by 15.4%; Surface hydrophilicity ↑; No change in salt rejection	2012 [30]
AgNPs	Polyelectrolytes	0.01 wt% for each layer	Hydrophilicity ↑; P_w↑ and MgCl2 rejection ↓; Strong TFNt-microbial property	2013 [16]
NaA zeolite NPs	PA	0.4% (w/v) in organic phase	Double the water permeability with equivalent salt rejection;	2007 [12]
Silica-NH_2 NPs	PA	0.03% (w/v) in aqueous phase	P_w ↑ by 40%; Na_2SO_4 rejection ↓	2012 [18]
SiO_2	PA	0.05% (w/v) in organic phase	P_w ↑ by 63.5 with constant NaCl rejection	2012 [24]
SiO_2	PA	0.05% (w/v) in organic phase	Pw ↑ by 15%; MgSO4 rejection ↑	2014 [45]
MWCNTs	Polyester	0.05% (w/v) in aqueous phase	P_w ↑ by 70%; Na_2SO_4 rejection ↑	2013 [18]
MWCNTs-NH_2	PA	0.005 wt% in PA at optimum	P_w ↑ by 30%; NaCl and Na_2SO_4 rejection ↓	2016 [49]
GO	PA	0.02% (w/v) in aqueous phase	Pw ↑; No change in salt rejection	2015 [50]
GO	PA	0.02% (w/v) in organic phase	Pw ↑ with slightly reduced NaCl rejection	2016 [22]

444 Note:

445 [a] A silver loading of 10% in polyamide was reported in these works. The detailed characterization of silver loading (mass of silver versus mass of polyamide) was available.

3.6. Conclusions

In this study, a PDA nano-template was used to prepare a substrate with high loadings of uniformly distributed AgNPs. The TFNt membrane formed on this substrate showed significantly enhanced separation performances (doubled water permeability, increased salt rejection to NaCl and $MgSO_4$, and enhanced NaCl/$MgSO_4$ selectivity) and antimicrobial properties compared to the TFC and the conventional TFN membranes. In contrast, the conventional TFN membrane prepared by blending AgNPs directly into the organic TMC phase for the interfacial polymerization suffered from a reduced salt rejection, which may be attributed to the agglomeration of AgNPs as well as the reduced crosslinking degree of the polyamide rejection layer. The preloading of AgNPs with the *in situ* reduction of silver ions by the PDA nano-template allows significantly higher silver loading (14.7 ± 2.2 μg/cm^2) in the TFNt compared to that in the conventional TFN (3.2 ± 0.4 μg/cm^2), which explains its better antibacterial performance.

Acknowledgement

The study receives financial support from the Innovation and Technology Commission of the Hong Kong Government (Project # ITS/208/14) and the General Research Fund of the Research Grants Council (Project # 17207514). The partial funding support from Strategic Research Theme on Clean Energy at the University of Hong Kong and the Seed Grant for Basic Research (104003453) are also appreciated.

Appendices

Appendix A. X-ray photoelectron spectroscopy and EDS results; Appendix B. Contact angle results; Appendix C. Membrane separation performance; Appendix D. Silver leaching tests; Appendix E. Dynamic antibiofouling test; Appendix F. Long term filtration test.

References

[1] B. Van der Bruggen, C. Vandecasteele, Removal of pollutants from surface water and groundwater by nanofiltration: overview of possible applications in the drinking water industry, Environ. Pollut., 122 (2003) 435-445.

[2] A. Seidel, M. Elimelech, Coupling between chemical and physical interactions in natural organic matter (NOM) fouling of nanofiltration membranes: implications for fouling control, J. Membr. Sci., 203 (2002) 245-255.

[3] K. Chon, J. Cho, H.K. Shon, Fouling characteristics of a membrane bioreactor and nanofiltration hybrid system for municipal wastewater reclamation, Bioresour. Technol., 130 (2013) 239-247.

[4] L.D. Nghiem, S. Hawkes, Effects of membrane fouling on the nanofiltration of pharmaceutically active compounds (PhACs): mechanisms and role of membrane pore size, Sep. Purif. Technol., 57 (2007) 176-184.

[5] W.J. Lau, A.F. Ismail, Polymeric nanofiltration membranes for textile dye wastewater treatment: Preparation, performance evaluation, transport modelling, and fouling control - a review, Desalination, 245 (2009) 321-348.

[6] T.-Y. Liu, Z.-H. Liu, R.-X. Zhang, Y. Wang, B. Van der Bruggen, X.-L. Wang, Fabrication of a thin film nanocomposite hollow fiber nanofiltration membrane for wastewater treatment, J. Membr. Sci., 488 (2015) 92-102.

[7] J. Lin, C.Y. Tang, W. Ye, S.-P. Sun, S.H. Hamdan, A. Volodin, C. Van Haesendonck, A. Sotto, P. Luis, B. Van der Bruggen, Unraveling flux behavior of superhydrophilic loose nanofiltration membranes during textile wastewater treatment, J. Membr. Sci., 493 (2015) 690-702.

[8] A.S. Al-Amoudi, A.M. Farooque, Performance restoration and autopsy of NF membranes used in seawater pretreatment, Desalination, 178 (2005) 261-271.

[9] Y. Song, B. Su, X. Gao, C. Gao, The performance of polyamide nanofiltration membrane for long-term operation in an integrated membrane seawater pretreatment system, Desalination, 296 (2012) 30-36.

[10] C.Y.Y. Tang, Y.N. Kwon, J.O. Leckie, Effect of membrane chemistry and coating layer on physiochemical properties of thin film composite polyamide RO and NF membranes I. FTIR and XPS characterization of polyamide and coating layer chemistry, Desalination, 242 (2009) 149-167.

[11] R.J. Petersen, Composite reverse osmosis and nanofiltration membranes, J. Membr. Sci., 83 (1993) 81-150.

[12] B.H. Jeong, E.M.V. Hoek, Y.S. Yan, A. Subramani, X.F. Huang, G. Hurwitz, A.K. Ghosh, A. Jawor, Interfacial polymerization of thin film nanocomposites: A new concept for reverse osmosis membranes, J. Membr. Sci., 294 (2007) 1-7.

[13] M.L. Lind, A.K. Ghosh, A. Jawor, X. Huang, W. Hou, Y. Yang, E.M. Hoek, Influence of zeolite crystal size on zeolite-polyamide thin film nanocomposite membranes, Langmuir, 25 (2009) 10139-10145.

[14] M.L. Lind, B.-H. Jeong, A. Subramani, X. Huang, E.M. Hoek, Effect of mobile cation on zeolite-polyamide thin film nanocomposite membranes, J. Mater. Res., 24 (2009) 1624-1631.

[15] H.S. Lee, S.J. Im, J.H. Kim, H.J. Kim, J.P. Kim, B.R. Min, Polyamide thin-film nanofiltration membranes containing TiO 2 nanoparticles, Desalination, 219 (2008) 48-56.

[16] X. Liu, S. Qi, Y. Li, L. Yang, B. Cao, C.Y. Tang, Synthesis and characterization of novel antibacterial silver nanocomposite nanofiltration and forward osmosis membranes based on layer-by-layer assembly, Water Res., 47 (2013) 3081-3092.

[17] J. Wu, C. Yu, Q. Li, Regenerable antimicrobial activity in polyamide thin film nanocomposite membranes, J. Membr. Sci., 476 (2015) 119-127.

[18] H.Q. Wu, B.B. Tang, P.Y. Wu, Optimizing polyamide thin film composite membrane covalently bonded with modified mesoporous silica nanoparticles, J. Membr. Sci., 428 (2013) 341-348.

[19] H. Wu, B. Tang, P. Wu, Optimization, characterization and nanofiltration properties test of MWNTs/polyester thin film nanocomposite membrane, J. Membr. Sci., 428 (2013) 425-433.

[20] K. Wong, P. Goh, B. Ng, A. Ismail, Thin film nanocomposite embedded with polymethyl methacrylate modified multi-walled carbon nanotubes for CO 2 removal, RSC Adv., 5 (2015) 31683-31690.

[21] C.-F. de Lannoy, D. Jassby, D. Davis, M. Wiesner, A highly electrically conductive polymer–multiwalled carbon nanotube nanocomposite membrane, J. Membr. Sci., 415 (2012) 718-724.

[22] J. Yin, G. Zhu, B. Deng, Graphene oxide (GO) enhanced polyamide (PA) thin-film nanocomposite

(TFN) membrane for water purification, Desalination, 379 (2016) 93-101.
[23] H.M. Hegab, L. Zou, Graphene oxide-assisted membranes: fabrication and potential applications in desalination and water purification, J. Membr. Sci., 484 (2015) 95-106.
[24] J. Yin, E.S. Kim, J. Yang, B.L. Deng, Fabrication of a novel thin-film nanocomposite (TFN) membrane containing MCM-41 silica nanoparticles (NPs) for water purification, J. Membr. Sci., 423 (2012) 238-246.
[25] L.X. Dong, X.C. Huang, Z. Wang, Z. Yang, X.M. Wang, C.Y. Tang, A thin-film nanocomposite nanofiltration membrane prepared on a support with in situ embedded zeolite nanoparticles, Sep. Purif. Technol., 166 (2016) 230-239.
[26] Z. Yang, Y. Wu, J. Wang, B. Cao, C.Y. Tang, In Situ Reduction of Silver by Polydopamine: A Novel Antimicrobial Modification of a Thin-Film Composite Polyamide Membrane, Environ. Sci. Technol., 50 (2016) 9543-9550.
[27] H. Guo, Y. Deng, Z. Yao, Z. Yang, J. Wang, C. Lin, T. Zhang, B. Zhu, C.Y. Tang, A highly selective surface coating for enhanced membrane rejection of endocrine disrupting compounds: Mechanistic insights and implications, Water Res., 121 (2017) 197-203.
[28] Z. Yang, J. Yin, B.L. Deng, Enhancing water flux of thin-film nanocomposite (TFN) membrane by incorporation of bimodal silica nanoparticles, Aims Environ. Sci., 3 (2016) 185-198.
[29] S.Y. Lee, H.J. Kim, R. Patel, S.J. Im, J.H. Kim, B.R. Min, Silver nanoparticles immobilized on thin film composite polyamide membrane: characterization, nanofiltration, antifouling properties, Polym Advan Technol, 18 (2007) 562-568.
[30] E.S. Kim, G. Hwang, M.G. El-Din, Y. Liu, Development of nanosilver and multi-walled carbon nanotubes thin-film nanocomposite membrane for enhanced water treatment, J. Membr. Sci., 394 (2012) 37-48.
[31] X. Liu, X. Jin, B. Cao, C.Y. Tang, Bactericidal activity of silver nanoparticles in environmentally relevant freshwater matrices: influences of organic matter and chelating agent, J. Environ. Chem. Eng., 2 (2014) 525-531.
[32] C.Y. Chen, G.W. Nace, P.L. Irwin, A 6 x 6 drop plate method for simultaneous colony counting and MPN enumeration of Campylobacter jejuni, Listeria monocytogenes, and Escherichia coli, J Microbiol Meth, 55 (2003) 475-479.
[33] B.A. Tarboush, D. Rana, T. Matsuura, H. Arafat, R. Narbaitz, Preparation of thin-film-composite polyamide membranes for desalination using novel hydrophilic surface modifying macromolecules, J. Membr. Sci., 325 (2008) 166-175.
[34] H. Lee, S.M. Dellatore, W.M. Miller, P.B. Messersmith, Mussel-inspired surface chemistry for multifunctional coatings, Science, 318 (2007) 426-430.
[35] G.-E. Chen, Y.-J. Liu, Z.-L. Xu, Y.-J. Tang, H.-H. Huang, L. Sun, Fabrication and characterization of a novel nanofiltration membrane by the interfacial polymerization of 1, 4-diaminocyclohexane (DCH) and trimesoyl chloride (TMC), RSC Adv., 5 (2015) 40742-40752.
[36] Y.F. Li, Y.L. Su, J.Y. Li, X.T. Zhao, R.N. Zhang, X.C. Fan, J.N. Zhu, Y.Y. Ma, Y. Liu, Z.Y. Jiang, Preparation of thin film composite nanofiltration membrane with improved structural stability through the mediation of polydopamine, J. Membr. Sci., 476 (2015) 10-19.
[37] J. Yin, B.L. Deng, Polymer-matrix nanocomposite membranes for water treatment, J. Membr. Sci., 479 (2015) 256-275.
[38] L. Tang, K.J. Livi, K.L. Chen, Polysulfone membranes modified with bioinspired polydopamine and silver nanoparticles formed in situ to mitigate biofouling, Environ. Sci. Technol. Lett., 2 (2015) 59-65.
[39] W.F. Chan, E. Marand, S.M. Martin, Novel zwitterion functionalized carbon nanotube nanocomposite membranes for improved RO performance and surface anti-biofouling resistance, J. Membr. Sci., 509 (2016) 125-137.
[40] K.A. Huynh, J.M. McCaffery, K.L. Chen, Heteroaggregation reduces antimicrobial activity of silver nanoparticles: evidence for nanoparticle–cell proximity effects, Environ. Sci. & Technol. Lett., 1 (2014) 361-366.
[41] E.J. Stuart, K. Tschulik, J. Ellison, R.G. Compton, Improving the Rate of Silver Nanoparticle Adhesion to ‘Sticky Electrodes’: Stick and Strip Experiments at a DMSA‐Modified Gold Electrode, Electroanalysis, 26 (2014) 285-291.
[42] M. Stevanović, I. Savanović, V. Uskoković, S.D. Škapin, I. Bračko, U. Jovanović, D. Uskoković, A new, simple, green, and one-pot four-component synthesis of bare and poly (α, γ, L-glutamic acid)-capped silver nanoparticles, Colloid Polym. Sci. , 290 (2012) 221-231.

[43] S. Dunn, S. Sharp, S. Burgess, The photochemical growth of silver nanoparticles on semiconductor surfaces—initial nucleation stage, Nanotechnology, 20 (2009) 115604.
[44] C. Zhang, Z. Hu, B. Deng, Silver nanoparticles in aquatic environments: Physiochemical behavior and antimicrobial mechanisms, **Water Res.**, 88 (2016) 403-427.
[45] Q. Li, Y.H. Wang, J. Song, Y.P. Guan, H. Yu, X.H. Pan, F.Y. Wu, M. Zhang, Influence of silica nanospheres on the separation performance of thin film composite poly(piperazine-amide) nanofiltration membranes, Appl Surf Sci, 324 (2014) 757-764.
[46] X. Yang, Y. Du, X. Zhang, A. He, Z.-K. Xu, Nanofiltration Membrane with a Mussel-Inspired Interlayer for Improved Permeation Performance, Langmuir, 33 (2017) 2318-2324.
[47] J.S. Kim, E. Kuk, K.N. Yu, J.H. Kim, S.J. Park, H.J. Lee, S.H. Kim, Y.K. Park, Y.H. Park, C.Y. Hwang, Y.K. Kim, Y.S. Lee, D.H. Jeong, M.H. Cho, Antimicrobial effects of silver nanoparticles, Nanomedicine, 3 (2007) 95-101.
[48] X. Qu, P.J. Alvarez, Q. Li, Applications of nanotechnology in water and wastewater treatment, Water Res., 47 (2013) 3931-3946.
[49] N. Zarrabi, M.E. Yekavalangi, V. Vatanpour, A. Shockravi, M. Safarpour, Improvement in desalination performance of thin film nanocomposite nanofiltration membrane using amine-functionalized multiwalled carbon nanotube, Desalination, 394 (2016) 83-90.
[50] S. Bano, A. Mahmood, S.-J. Kim, K.-H. Lee, Graphene oxide modified polyamide nanofiltration membrane with improved flux and antifouling properties, J. Mater. Chem. A, 3 (2015) 2065-2071.